High Speed SRM Using Vector Control for Electric Vehicle

Kohei Aiso, and Kan Akatsu *Member, IEEE*

Abstract—The high speed motor is effective to realize downsizing motor in an electric vehicle (EV). Switched Reluctance Motor (SRM) is possible to the high speed drive because the rotor structure has simple and robust. However, the vibration and the acoustic noise are large from the drive principle. Moreover, the conventional complicated current excitation results in the difficulty of the torque controller design. To overcome these problems, the vector control has been proposed for SRM drive. However, the vector control has not been applied to the SRM in the high speed drive. In this paper, the drive conditions such as switching frequency, bus voltage for driving the SRM in the high speed region are clarified. It is shown that the proposed SRM can be driven by the vector control in the high speed region and can realize low vibration.

Index Terms— Switched reluctance motor, Vector control, high speed drive.

I. Introduction

ELECTRIC vehicles (EVs) have become popular as one of energy saving countermeasures. For EV's traction motors, the downsizing a motor system is required to improve the electric power consumption and keep the effective space in the motor room. One of the methods to downsize the motor volume is to increase the motor speed [1]. The output power of motors is defined as the product of torque and rotation speed. The downsizing can be realized by increasing the rotation speed, while obtaining the same output power. Therefore, Permanent Magnet Synchronous Motors (PMSMs) using rare earth magnets are representative for EV's traction motor because they achieve the high torque density and high efficiency. However, PMSMs have several disadvantages. The rare earth metals used in the rotor need the high manufacturing cost. Moreover, the high speed drive is limited because the mechanical strength is low due to the permanent magnet in the rotor.

Switched Reluctance Motors (SRMs) have been expected as an alternative for PMSMs [2]. SRMs have the salient pole structure in the stator and the rotor, and only constructed by the iron core and the winding. Therefore, SRMs have simple and robust structure and it is suitable to drive in the high speed

region. They can achieve the high output power and the downsizing of the motor volume by the high speed rotation. Therefore, various SRMs for traction's motor have been reported. The SRM was designed by using low-iron-loss steel, 0.1-mm thick high-silicon steel to achieve the high efficiency, high torque density and a 50 kW output power from 1200 to 6000 r/min, as same dimension of the PMSM used in the second-generation Toyota Prius [3]. The 80kW SRM with amorphous steel sheet for realizes the high output power and the downsizing of motor volume by driving in more high speed region 30000 rpm compared with PMSMs. Moreover, the high efficiency can be obtained by reducing the iron loss owing to use amorphous steel sheet [4]. Also, 12/26 pole SRM with high specific torque has been proposed for in-wheel EV application [5]. The SRM which are composed by the segmented outer rotor structure and the concentrated-winding arrangement has realized the downsizing of motor volume and high efficiency by decreasing the end-winding volume and the copper loss.

However, SRMs have several disadvantages due to the conventional driving method. In general, SRMs are driven by the unipolar current. The current excitation starts around position where the rotor pole begins to align with the stator pole and continues at constant level by using the hysteresis control or the voltage single pulse drive. Then, it is eliminated before the rotor pole completely aligns with the stator pole. Consequently, the discontinuous unipolar current excitation is often applied to the SRM drive. The discontinuous current excitation results in the large vibration and acoustic noise in the SRMs. Especially, the large vibration is generated by changing the radial force between the rotor pole and the stator pole when the voltage instantaneously turned off [6][7]. The driving method to reduce the vibration have been reported [8][9]. In addition, the complicated unipolar current excitation results in the difficulty of the torque controller design. The simultaneous optimization process for some controlled parameters such as the turn-on angle, turn-off angle, and current chopping level is inevitable [10][11]. Considering variable speed applications, these parameters must be optimized for each drive condition to achieve the demand torque, high motor efficiency, wide driving range, and low vibration.

To overcome these problems, a vector control for SRM has been proposed [12][13]. In the vector control of SRM, sinusoidal current with a DC offset is applied to each circuit as the unipolar excitation current. The excitation current consists of the DC and AC components. These components generate the

Kohei Aiso is an assistant professor at department of electrical engineering and bio science, school of advanced science and engineering, Waseda University, Tokyo, Japan.(e-mail: nb15101@shibaura-it.ac.jp, kaiso@aoni.waseda.jp).

Kan Akatsu is the professor in Yokohama National University.(e-mail: akatsu-kan-py@ynu.ac.jp).
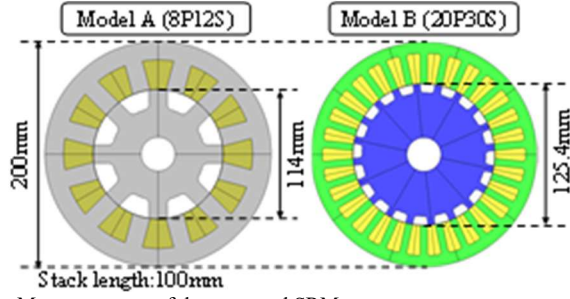
Fig.1. Motor structure of the proposed SRMs.

TABLE I
SPECIFICATION OF PROPOSED SRM

	Model A	Model B
Pole / Slot	8 / 12	20 / 30
Output power [kW]	85	34
Maximum speed [rpm]	50000	20000
Air gap length [mm]	0.5	0.5
Number of turns [turn/teeth]	5	5
Diameter of coil [mm]	6.0	4.0
Resistance [Ω/phase]	0.003	0.018
Core material	-	20H1200

Fig. 2. Self-inductance waveforms of the proposed SRMs.

Fig. 3. Current-Torque characteristic.

virtual rotor flux and rotating stator field, hence the SRM can be driven in the same way as conventional AC machines. Moreover, it has been shown that the vibration and the acoustic noise of the SRM can be reduced by the continuous current excitation in the vector control. However, the vector control has not been applied to the SRM driven in the high speed region because the bus voltage, the switching frequency, and the specification of inverter to realize the vector control in high speed drive have not been clarified.

In this research, drive conditions such as the bus voltage, switching frequency for applying vector control to the SRM in high speed drive is clarified. Moreover, it is verified by the experiment that the proposed SRM can be driven by the vector control in the high speed region and can realize the high output power and low vibration. The final targets are to evaluate the 8-pole 12-slot SRM that satisfies the maximum rotation speed 50000rpm and the rated output power of 85kW and to drive it by vector control. However, the maximum rotation speed is limited to 20000rpm by the experimental environment. Therefore, this paper proposes the 20-pole 30-slot SRM driven in 20000rpm which has same electrical frequency for the 8-pole 12-slot SRM driven in 50000rpm, performances of the proposed SRM in vector control are evaluated.

II. PROPOSED SRM

The 8 pole 12 slot SRM (model A) which satisfies the maximum rotation speed 50000rpm and the 20 pole 30 slot SRM (model B) which satisfies the maximum rotation speed 20000rpm are shown in Fig. 1 and specifications are shown in Table I. As shown in Fig. 1 and Table I, the 20 pole 30 slot SRM is designed to same electrical angular frequency and electrical characteristics for 8 pole 12 slot SRM to evaluate the controllability under the high speed rotation. The electrical frequency at the maximum rotation is expressed as follow:
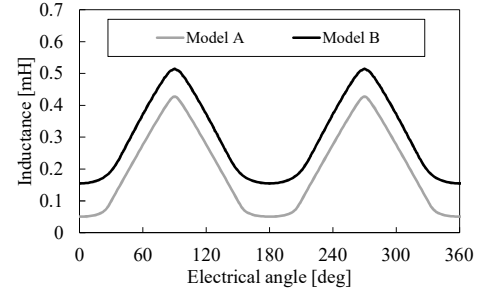
$$f_m = N_m \times \frac{P}{60} \qquad (1)$$
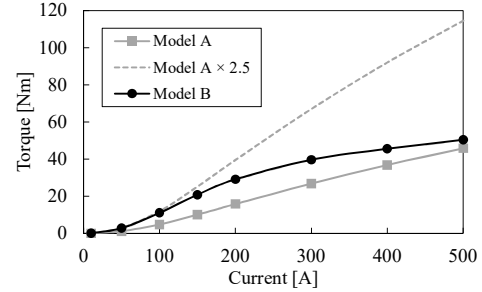
where f_m is the maximum electrical frequency, N_m is the maximum rotation speed, P is the number of pole. As shown in (1), the maximum electrical frequency is 6.67kHz in the model A. In model B, the number of pole 20 is determined so that the maximum electrical frequency at the maximum rotation speed 20000rpm is equal to model A. These two SRMs have the same outer diameter, stack length and air gap length. In addition, as shown in Fig. 2, they are designed so that the variation of their self-inductance distribution are almost equal. The torque of SRMs is expressed as follow:

$$T = \frac{P}{2} \frac{\partial L}{\partial \theta} i^2 \qquad (2)$$

where T, L, θ and i are output torque, inductance, electric angle and phase current, respectively. As shown in (2), when the same current value is supplied to them, the output torque is proportional to the number of poles. Therefore, the torque of model B is 2.5 times that of model A. On the other hand, the required current of model B is 0.63 times that of model A to obtain same torque. Fig. 3 shows the current-torque characteristics. As shown in Fig. 3, the torque of model B is 2.5 times that of model A in no magnetic saturation area of low current by applying same current.

III. CONTROLLABILITY OF VECTOR CONTROL FOR SRM

A. Principle and current controller of vector control

Fig. 4 shows the vector control of SRM. A three-phase sinusoidal current including DC offset is supplied as an excitation current. The AC component produces a rotating magnetic field in the stator. The DC component produces a rotating magnetic flux vector depending on the rotor position. This magnetic flux vector can be regarded virtually as the rotor field magnetic flux. From these reasons, torque is generated by the interaction between the rotating magnetic field in the stator
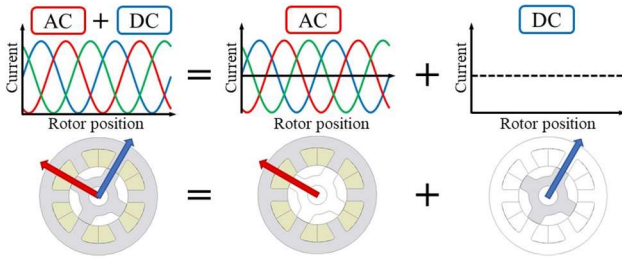
Fig. 4. Vector control of SRM.

and the magnetic flux in the rotor.

The torque generation in the vector control of the SRM is discribed by the mathematical formula [9][10]. The voltage equation of the equivalent SRM is expressed by d-q axis and zero-phase.

$$
\begin{bmatrix} v_d \\ v_q \\ v_0 \end{bmatrix} = R \begin{bmatrix} i_d \\ i_q \\ i_0 \end{bmatrix} + \begin{bmatrix} L_{dc} & 0 & L_{ac}/\sqrt{2} \\ 0 & L_{dc} & 0 \\ L_{ac}/\sqrt{2} & 0 & L_{dc} \end{bmatrix} \left(p \begin{bmatrix} i_d \\ i_q \\ i_0 \end{bmatrix} \right)
$$
$$
+ 2\omega \begin{bmatrix} 0 & -L_{dc} & 0 \\ L_{dc} & 0 & L_{ac}/\sqrt{2} \\ 0 & 0 & 0 \end{bmatrix} \begin{bmatrix} i_d \\ i_q \\ i_0 \end{bmatrix}
\tag{3}
$$

where v_d, v_q, v_0, i_d, i_q, i_0, R, L_{dc}, and L_{ac} are the d-axis voltage, q-axis voltage, zero-phase voltage, the d-axis current, q-axis current, zero-phase current, winding resistance, DC component of the self-inductance, and amplitude of the self-inductance, respectively. As shown in (3), the zero-phase component is calculated from the DC component of the excitation current. Given the inductance matrix of the second term of (3), the virtual rotor flux is derived from the following equation:

$$
\Phi_r = \frac{L_{ac}}{\sqrt{2}} i_0
\tag{4}
$$

where Φ_r is the virtual rotor flux. That is, as shown in (4), the virtual rotor flux is produced by the zero-phase current. Then, the torque of SRM is expressed as follow:

$$
T = 2P\Phi_r i_q
\tag{5}
$$

$$
T = \sqrt{2} P L_{ac} i_0 i_q .
\tag{6}
$$

(4) and (5) describes that the zero-phase and q-axis currents are equivalent to the rotor flux and torque currents, respectively. From (4), (5), the vector control system for SRM drive is shown in Fig. 5.
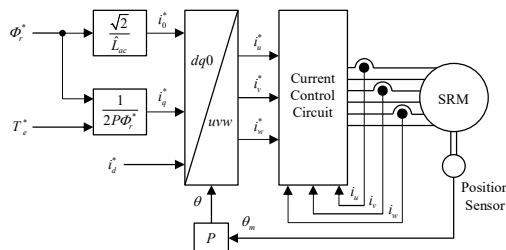

Fig. 5. Vector control system for SRM drive.

The current controller was described in [13]. Fig. 6 shows the current controller for the vector control. As shown in Fig. 6, there are three control parts: current PI, decoupling, and feed-forward controllers. The voltage commands from these controllers can be achieved by a carrier-based PWM inverter. The PI controller is used for the current regulation of each axis and phase component. The transfer function is expressed as follow:

$$
G_{PI}(s) = K_c \left(1 + \frac{1}{\tau_c s} \right)
\tag{7}
$$

where G_{PI}, K_c, and τ_c are the transfer function, gain, and time constant of the PI controller, respectively. Because of the decoupling and feed-forward controllers, the controlled-SRM can be identified as the RL circuits on the rotating reference frame. To achieve the ideal one-order current response, τ_c is set at the time constant of the controlled machine (i.e. L_{dc}/R). The gain K_c is designed depending on the current response speed. The current controller is used in the simulation and experiment in this paper.
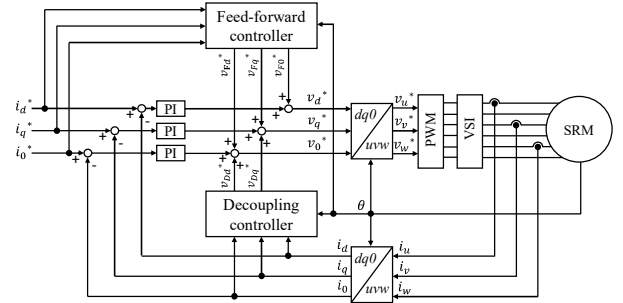

Fig. 6. Current controller for vector control.

B. Controllability of high speed drive

The switching frequency and the bus voltage for the demand output power and the rotation speed 20000rpm are considered. Current waveform and torque waveform for the switching frequency are evaluated by the simulation under the condition of the rotation speed 20000rpm, the reference torque 16.2 Nm. Fig. 7 shows the current waveform and torque waveform for the switching frequency. The switching frequency is changed and the total harmonic distortion and the current ripple ratio are calculated as follow.

$$
\text{THD} = \frac{\sqrt{I_2^2 + I_3^2 + I_4^2 + \cdots + I_n^2}}{I_1} \times 100[\%]
\tag{8}
$$

$$
\text{CRR} = \frac{i_{\max} - i_{\min}}{I_{ave}} \times 100[\%]
\tag{9}
$$

where THD is the total harmonic distortion, CRR is the current ripple ratio, $I_1 \ldots I_n$ are the effective value of each order harmonic current. i_{max}, i_{min}, i_{ave} are the maximum amplitude of current, the minimum amplitude of current, and the average of current, respectively. Table II shows the THD and the current ripple ratio of the q-axis and zero-phase for the switching frequency. As shown in Fig. 7 and Table II, the THD and the current ripple ratio are lower as increasing the switching frequency. The THD should be reduced as possible because the iron loss increase by harmonic fluxes in the high speed drive.
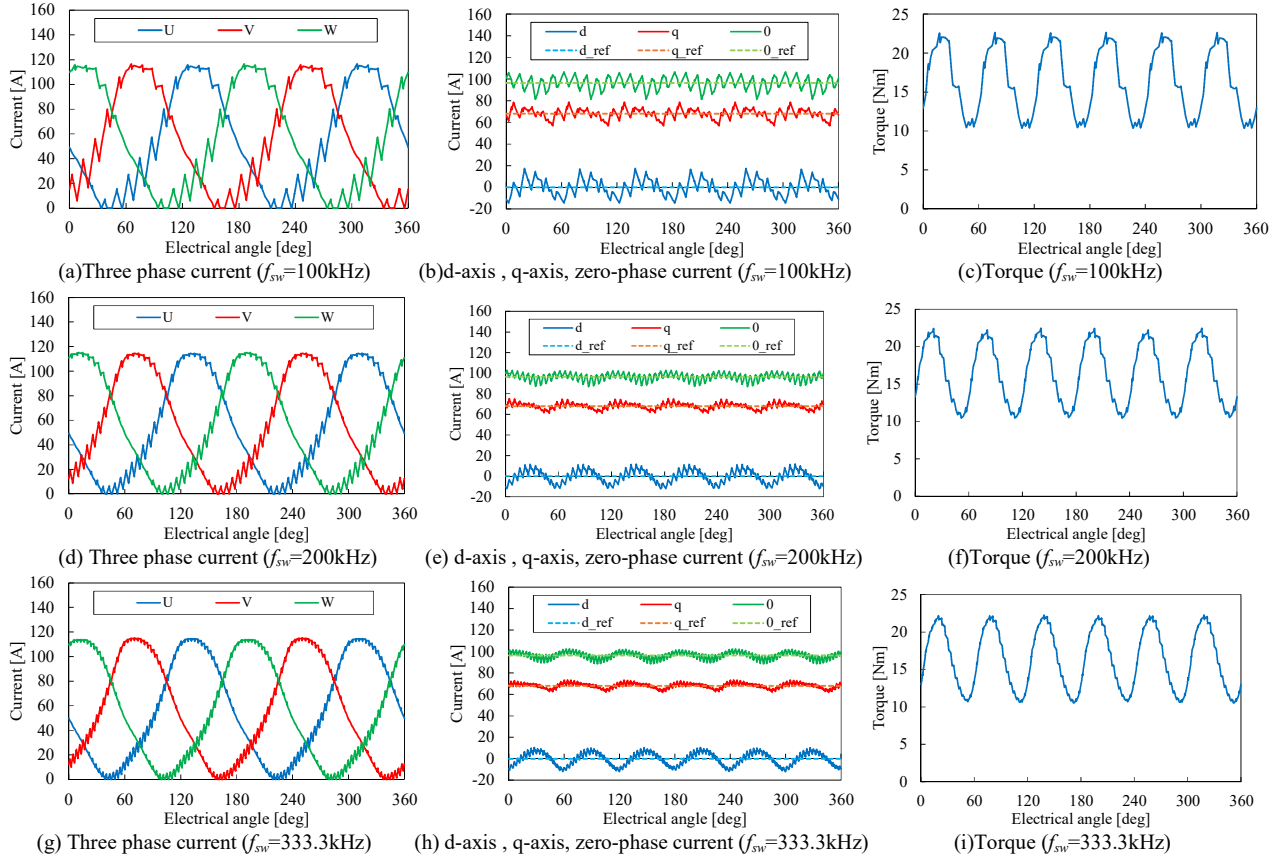
Fig. 7. Current waveform and torque waveform depending on switching frequency.

(a)Three phase current (f_{sw}=100kHz) (b)d-axis , q-axis, zero-phase current (f_{sw}=100kHz) (c)Torque (f_{sw}=100kHz)

(d) Three phase current (f_{sw}=200kHz) (e) d-axis , q-axis, zero-phase current (f_{sw}=200kHz) (f)Torque (f_{sw}=200kHz)

(g) Three phase current (f_{sw}=333.3kHz) (h) d-axis , q-axis, zero-phase current (f_{sw}=333.3kHz) (i)Torque (f_{sw}=333.3kHz)

TABLE II
THD AND CURRENT RIPPLE RATIO

Switching frequency [kHz]	100	200	333.3
3phase current THD [%]	15.3	11.1	10.5
q-axis current ripple ratio [%]	32.2	21.0	17.2
zero-phase current ripple ratio [%]	26.3	16.6	14.7

TABLE III
BUS VOLTAGE FOR TORQUE REFERENCE

Torque reference [Nm]	DC voltage [V]	300	400	500	600	700	800	900	1000
	Output torque [Nm]	4.04	4.95	5.05	5.08	-	-	-	-
5	Current [Arms]	37.47	37.82	37.77	37.81	-	-	-	-
	Modulation rate	5.11	1.33	0.99	0.83	-	-	-	-
	Output torque [Nm]	-	6.53	9.71	10.01	10.14	10.18	-	-
10	Current [Arms]	-	50.57	53.80	53.58	53.53	53.55	-	-
	Modulation rate	-	7.88	1.79	1.20	0.99	0.88	-	-
	Output torque [Nm]	-	-	10.15	15.64	16.11	16.22	16.38	16.38
16.2 (34kW, 20000rpm)	Current [Arms]	-	-	63.38	69.27	68.46	68.08	68.40	68.18
	Modulation rate	-	-	8.62	2.24	1.36	1.10	0.98	0.89

TABLE IV
SPECIFICATION OF SiC INVERTER

Rated capacity [kVA]	50
Rated AC output current [Arms]	72.2
Rated AC input voltage [V]	700
Maximum switching frequency [kHz]	200

The decrease ratio of THD is high between 100kHz and 200kHz of the switching frequency. On the other hand, it is not so changed in more than 200kHz of switching frequency. The current ripple and THD become an acceptable value by setting the number of switching per one electrical angle period to 30 times or more. So, the required switching frequency is expressed as follow:

$$f_{sw} = f_m \times 30 = 200 \text{ [kHz]} \tag{10}$$

where f_{sw} is the switching frequency.

The bus voltage required for the realizing torque reference is considered by the simulation. As the simulation condition, the rotation speed is 20000rpm and the switching frequency is 200

kHz. The simulation result is shown in Table III. As shown in Table III, the vector control is possible in the area that the modulation ratio is less than 1.0. In the area that the modulation ratio is more than 1.0, the vector control shifts to the single pulse drive. Therefore, the bus voltage is required to achieve less than modulation ratio 1.0 for the vector control. The bus voltage becomes higher for the vector control as increasing the reference torque. The bus voltage 900V is required to achieve the 16.2Nm, 34kW. From these simulation results, the SiC inverter is selected to satisfy the high switching frequency for the vector control in the high speed region. The specification of inverter is shown in Table IV. As shown in Table IV, the rated power is 50kVA, the rated AC output current 72.2Arms, the rated DC input voltage 700V, the maximum switching frequency is 200kHz.

IV. EXPERIMENT RESULTS

A prototype machine of the proposed SRM is evaluated and compared with the simulation results of the Finite Element Analysis (FEA). Fig. 8 shows the prototype SRM and Fig. 9 shows the experiment set-up. As shown in Fig. 9, the performances of prototype SRM are evaluated by the dynamometer. The asymmetric H-bridge inverter is constructed by using two three-phase half bridge SiC inverters.
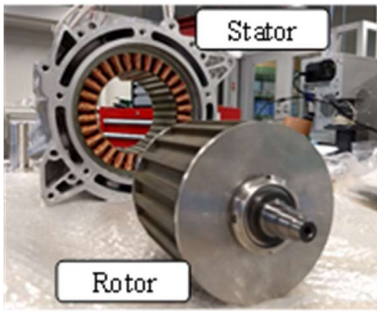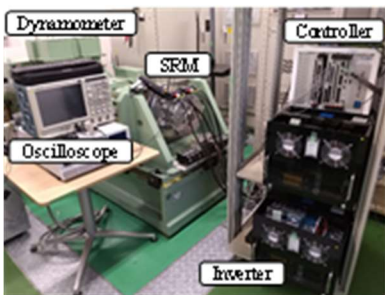

Fig. 8. Prototype SRM.

Fig. 9. Experimental set-up.

A. Performances of prototype motor

The inductance and current-torque characteristic are measured. Fig. 10 shows the inductance waveform. The inductance waveform is measured under applying DC current 10A to the U-phase coil. As shown in Fig. 10, although the measured inductance value is higher than that of the simulation result, the inductance variation almost corresponds to that of the simulation result. The DC component of the inductance L_{dc} in FEA and the experiment are 0.30mH, and 0.32mH. The fundamental AC component of the inductance L_{ac} in FEA and

experiment are 0.17mH, and 0.14mH. As shown in (7), the time constant of PI controller τ_c is set by the phase resistance R and the DC component of inductance L_{dc} in the experiment. The L_{ac} and L_{dc} of inductance parameters are used as a constant since the SRM is controlled by the vector control. From the static inductance, it is expected that the prototype SRM has same torque characteristic for the simulation.

Fig. 11 shows the current-torque characteristic. The current-torque characteristic is measured under the condition of the rotation speed 500rpm, hysteresis control drive, bus voltage 100V, turn-on angle 0 degree, turn-off angle 80 degree. As shown in Fig. 10, the current-torque characteristic correspond to that of the simulation result.
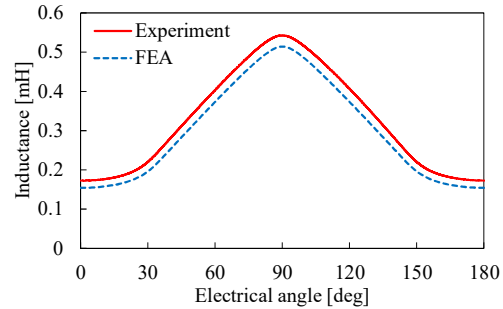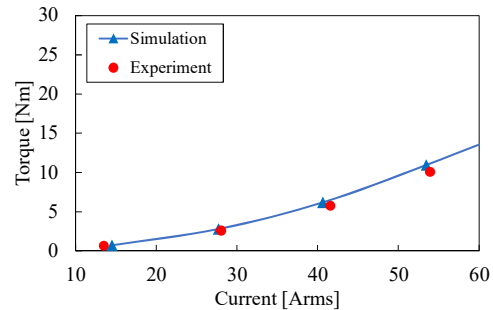

Fig. 10. Inductance waveform.

Fig. 11. Current-torque characteristic.

B. Control precision for the vector control

The torque control precision is verified. The output torque is measured under the condition of the rotation speed 500rpm, vector control, bus voltage 100V, switching frequency 200kHz, and torque command (5Nm, 10Nm, 15Nm). Fig. 12 shows the output torque for the reference torque. As shown in Fig. 12, it is confirmed that the output torque corresponds the torque commands. The vector control can achieve the desired mean torque in the SRM drive. Fig. 13 shows the output current for each reference torque. As shown in Fig. 13, as described in section III, a three-phase sinusoidal current including DC offset is supplied as an excitation current to achieve each demand torque. The AC and DC components of the measured current almost correspond to the simulation results.

C. Controllability in maximum rotation speed

The controllability of vector control is verified under the condition of the maximum rotation speed 20000rpm, vector control, bus voltage 300V, switching frequency 200kHz, and no load. Fig. 14 shows the output current in the maximum rotation speed 20000rpm. As shown in Fig. 14, these currents of the experiment and the simulation have similar waveforms and it is
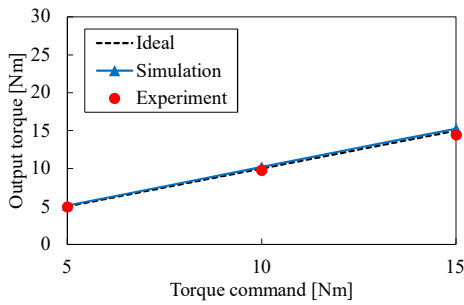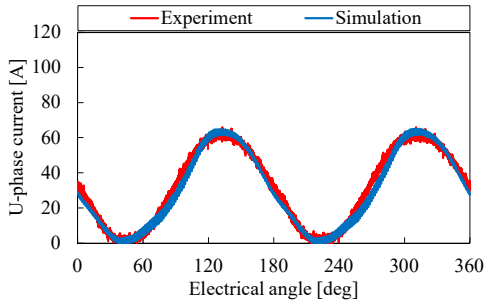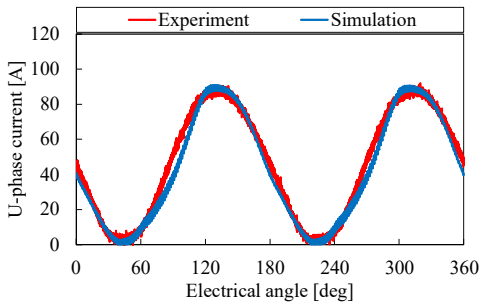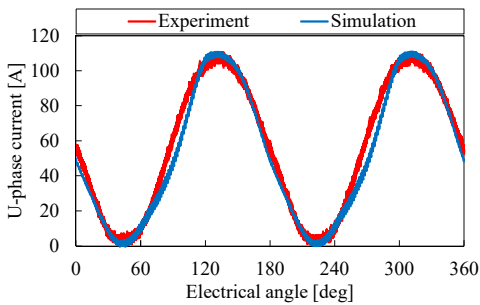
Fig. 12. Torque control precision.

(a) Torque command (5Nm)

(b) Torque command (10Nm)

(c) Torque command (15Nm)

Fig. 13. Comparison of output current.

confirmed that the SRM can be driven by the vector control atthe maximum rotation speed 20000rpm. That is, it means that the 8-pole 12-slot SRM can be driven in 50000rpm by the vector control.

D. Vibration of motor

The vibration acceleration of the SRM is measured in the vector control and the conventional single pulse drive. The position of acceleration sensor in the motor is shown in Fig. 16 and the drive conditions are (5000rpm, 14Nm) and (10000rpm, 10Nm). Fig. 16 shows the comparison of the vibration acceleration and Fig. 17 shows the comparison of the current

waveforms. The fundamental frequency of the excitation in the three phase SRM is 5kHz(5000rpm), 10kHz(10000rpm). As shown in Fig. 16, the vibration acceleration is large at the fundamental frequency of the excitation. The vibration acceleration in the vector control is lower than that of the single pulse drive. In the vector control, it is confirmed that the vibration acceleration can be reduced due to be small the changing of the radial force by the continuous and smooth current excitation.
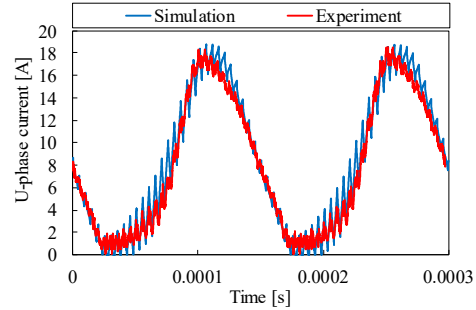

Fig. 14. Output current in the maximum rotation speed 20000rpm.
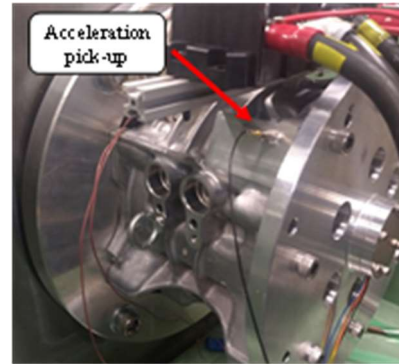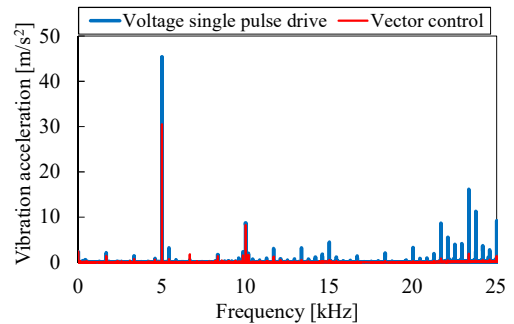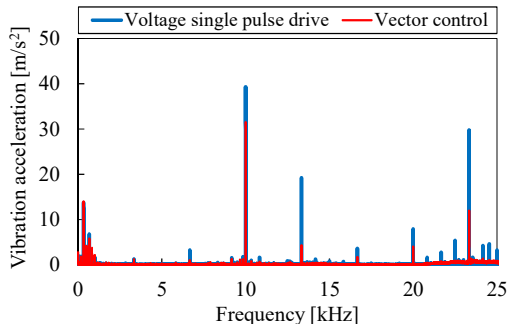

Fig. 15. Position of acceleration sensor in the motor.

(a) 5000rpm, 14Nm

(b) 10000rpm, 10Nm

Fig. 16. Comparison of the vibration acceleration.

(a) Single pulse drive (5000rpm, 14Nm)

(b) Single pulse drive (10000rpm, 10Nm)

(c) Vector control (5000rpm, 14Nm)
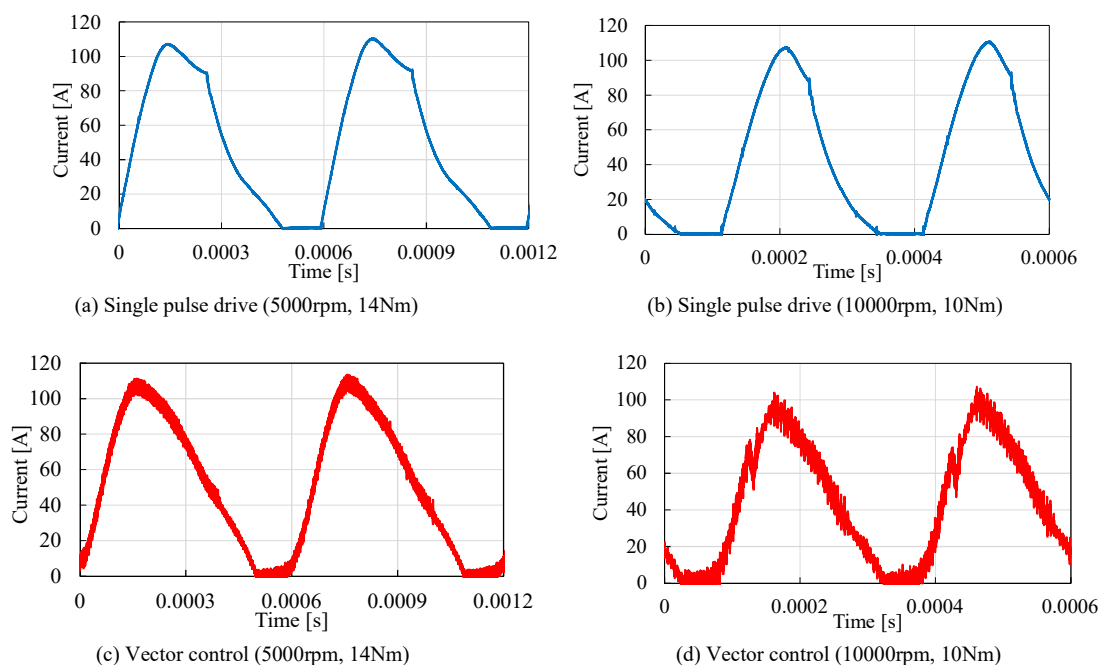
(d) Vector control (10000rpm, 10Nm)

Fig. 17. Comparison of the output current.

V. CONCLUSION

In this paper, to apply the vector control to the SRM in the high speed drive, the 20-pole 30-slot SRM driven in 20000rpm which has same electrical angular frequency for the 8-pole 12-slot SRM driven in 50000rpm was designed and evaluated. As a result of analysis, the proposed motor satisfied the demand performances such as torque and output power in the vector control by using the SiC inverter which has the switching frequency 200kHz. In the experiment, it was clarified that the proposed SRM can be driven by the vector control at the maximum rotation speed 20000rpm. That is, it means that the 8-pole 12-slot SRM can be driven in 50000rpm by the vector control. Finally, it was shown that the vibration of SRM can be reduced in the high speed region by applying the vector control compared with that in the conventional single pulse drive.

REFERENCES

[1] M. Besharati, J. Widmer, G. Atkinson, V. Pickert, Jamie Washington : "Super-high-speed switched reluctance motor for automotive traction", in *Proc. of IEEE Energy Conversion Congress and Exposition (ECCE)*, pp.5241-5248, Sept. 2015.

[2] Earl W. Fairall, Berker Bilgin, Ali Emadi : "State-of-the-Art High-speed Switched Reluctance Machines", *IEEE International Electric Machines and Drives Conference (IEMDC)*, pp.1621-1627, May 2015.

[3] A. Chiba, K. Kiyota, N. Hoshi, M. Takemoto, S. Ogasawara, "Development of a Rare-Earth-Free SR Motor with High Torque Density for Hybrid Vehicles", *IEEE Transactions on Energy Conversion*, vol.30, no.1, pp.175-182, Mar. 2015.

[4] K. Ueta, K. Akatsu, "Study of high-speed SRM with amorphous steel sheet for EV", in *Proc. of 19th International Conference on Electrical Machines and Systems 2016 (ICEMS 2016)*, Feb. 2017.

[5] S. P. Nikam, V. Rallabandi, B. G. Fernandes, "A High-Torque-Density Permanent-Magnet Free Motor for in-Wheel Electric Vehicle Application" *IEEE Transaction on Industry Application*, vol. 48, no. 6, pp.2287-2295, Nov. 2012.

[6] M. N. Answar and Iqbal Husain, "Radial Force Calculation and Acoustic Noise Prediction in Switched Reluctance Machines" *IEEE Transaction on Industry Application*, vol. 36, no. 6, pp.1589-1597, 2000.

[7] Chenjie Lin and Babak Fahimi, "Prediction of Radial Vibration in Switched Reluctance Machines", *IEEE Transaction on Energy Conversion*, vol. 29, no. 1, pp.250-258, 2014

[8] H. Makino, T. Kosaka, Nobuyuki Matsui, "Digital PWM-Control-Based Active Vibration Cancellation for Switched Reluctance Motors", *IEEE Transaction on Industry Application*, vol.51, no.6, pp.4521-4530, Nov. 2015.

[9] A. Tanabe, K. Akatsu, "Vibration reduction method in SRM with a smoothing voltage commutation by PWM", in *Proc. of 9th International Conference on Power Electronics and ECCE Asia (ICPE-ECCE Asia)*, June 2015.

[10] K. M. Rahman, B. Fahimi, G. Suresh, A. V. Rajarathnam, and M. Ehsani, "Advantages of Switched Reluctance Motor Applications to EV and HEV: Design and Control Issues," *IEEE Transactions on Industry Applications*, vol. 36, No. 1, pp. 111-121, January/February, 2000.

[11] I. Husain and S. A. Hossain, "Modeling, Simulation, and Control of Switched Reluctance Motor Drives," *IEEE Transactions on Industrial Electronics*, vol. 52, no. 6, pp. 1625-1634, December 2005.

[12] N. Nakao, K. Akatsu, "Vector control specialized for switched reluctance motor drives", *Proc. of International Conference on Electrical Machines (ICEM)*, pp.943-949, September 2014.

[13] N. Nakao, K. Akatsu, "Vector control for switched reluctance motor drives using an improved current controller", in *Proc. of IEEE Energy Conversion Congress and Exposition (ECCE)*, pp.1379-1386, Sept 2014.W.-K. Chen, *Linear Networks and Systems*. Belmont, CA: Wadsworth, 1993, pp. 123–135.

Kohei Aiso received B.S., M.S., and Ph. D degrees in electrical engineering from Shibaura Institute of Technology, Tokyo, Japan, in 2013, 2015, 2019 respectively. From 2019, he is an assistant professor at department of electrical engineering and bio science, school of advanced science and engineering, Waseda University, Tokyo, Japan. His current research focuses on motor design, motor control, and magnetic gear.

Kan Akatsu received B.S., M.S., and Ph. D degrees in electrical engineering from Yokohama National University, Yokohama, Japan, in 1995, 1997, 2000 respectively.

He joined Nissan Research Center, Yokosuka, Japan, in 2000, he contributed to the design and analysis of the new concept permanent magnet machines. In 2003, he joined the department of Electrical and Electric Engineering at Tokyo University of Agriculture and Technology, Tokyo, Japan, as an assistant professor. From 2005 to 2007, he is a JSPS Postdoctoral Fellowship for Research Abroad, visiting professor in WEMPEC (Wisconsin Electric Machines and Power Electronics Consortium), University of Wisconsin-Madison. From 2009, he was an associate professor, and he was a full professor in Shibaura Institute of Technology, Tokyo, Japan. From October 2019, he is a professor in Yokohama National University.

He is a committee member in IEEJ-IAS, a chair of International Affairs of IEEJ-IAS.